



Natural convection heat transfer between a body and its spherical enclosure
by Norman Weber

A thesis submitted to the Graduate Faculty in partial fulfillment of the requirements for the degree of
DOCTOR OF PHILOSOPHY in Aerospace and Mechanical Engineering
Montana State University
© Copyright by Norman Weber (1971)

Abstract:

Natural convection heat transfer between isothermal vertically eccentric spheres and centrally located vertical cylinders and their isothermal spherical enclosure was experimentally investigated. Pertinent dimensionless parameters and variables utilized in the investigation were Rayleigh number, based on gap width, N , Prandtl number, N_{PR} , eccentricity to gap width ratio, $e/(r - r_i)$, gap width to inner radius ratio, L/r , and aspect ratio, $H/2r$, and covered the following ranges: $4.7 < N_{PR} < 4148$, $4 \times 10^2 < N_{RA} < 9 \times 10^7$, $0.09 < L/r_i < 1.18$ and $-0.75 < e/(r_o - r_i) < +0.75$ for the eccentric — spheres; $6 < N_{pr} < 14$, $3.5 \times 10^3 < N_{ra} < 2.2 \times 10^8$, $1.14 < H/2r_i < 2.00$ $r_o - r_i$ and $0.09 < \text{-----} < 1.18$ for the vertical cylinder.

— r . — i Examination of the experimental data showed that the eccentricity had a slight effect on the average heat transfer coefficient. The negative eccentricities were found to produce slightly higher average heat transfer coefficients than positive eccentricities. The largest eccentricities, either positive or negative, were also seen to produce heat transfer coefficients larger than the next lower eccentricity, i.e., the average heat transfer coefficient for $e/(r_o - r_i) = \pm 0.75 >$ the average heat transfer coefficient for $e/(r - r_i) = \pm 0.50$, etc. Gap thickness to inner radius ratio, L/r_i was also found to have an effect on the average heat transfer coefficient. The larger values of L/r were found to yield higher values of Nusselt number. An increase in the viscosity did tend to suppress this behavior, however, the same trend was still found to exist. Heat transfer correlations for each individual fluid, as well as an overall correlation, were obtained for the eccentric sphere configuration utilizing conformal mapping techniques to transform the eccentric sphere configuration. Temperature profiles at five angular locations ($\theta = 0^\circ$, 40° , 80° , 120° , and 160°) were taken and yielded some insight as to the flow behavior and heat transfer as a result of eccentricity. A negative eccentricity was seen to enhance the convective activity while a positive eccentricity seemed to suppress the convective activity. A multicellular flow field is postulated for the smallest diameter ratio configuration.

The experimental data for the cylinders were examined independently and showed that aspect ratio did have an effect on the average heat transfer coefficient. The smaller aspect ratios for each diameter ratio produced higher average heat transfer coefficients. Heat transfer correlations were obtained for each cylinder as well as an overall heat transfer correlation for all of the cylinders. Temperature profiles were taken and were enlightening as to the nature of the effect of aspect ratio and diameter ratio on the flow field. The larger aspect ratios for all diameter ratios seemed to curtail the convective activity while the smaller aspect ratios for all diameter ratios seemed to promote convective activity. A multicellular flow regime is postulated for the smallest diameter ratio cylinder investigated.

NATURAL CONVECTION HEAT TRANSFER BETWEEN
A BODY AND ITS SPHERICAL ENCLOSURE

by

NORMAN WEBER

A thesis submitted to the Graduate Faculty in partial
fulfillment of the requirements for the degree

of

DOCTOR OF PHILOSOPHY

in

Aerospace and Mechanical Engineering

Approved:

W. Bishop
Head, Major Department

R. C. Powe
Chairman, Examining Committee

Henry J. Parsons
Graduate Dean

MONTANA STATE UNIVERSITY
Bozeman, Montana

December, 1971

ACKNOWLEDGMENT

The author wishes to express his sincere thanks and appreciation to all those that aided him in this effort. Special thanks are due to Dr. R. E. Powe, Dr. E. H. Bishop, and Dr. J. A. Scanlan for their advice, guidance, and understanding. Also, a special note of gratitude and thanks are due Gordon Williamson, who patiently constructed the entire apparatus. The writer is also very appreciative of the patience, understanding and sacrifices of Sophia, Kristen, Eric, and Tanya, his family.

This work was carried out through the support of the Atomic Energy Commission under Contract Number AT(45-1)-2214.

TABLE OF CONTENTS

Chapter	Page
VITA	ii
ACKNOWLEDGMENT	iii
LIST OF TABLES	v
LIST OF FIGURES	vi
ABSTRACT	x
NOMENCLATURE	xii
I. INTRODUCTION	1
II. LITERATURE REVIEW	6
III. EXPERIMENTAL APPARATUS AND PROCEDURE	35
IV. DISCUSSION OF RESULTS	55
V. CONCLUSION	131
APPENDIX I. COMPUTER PROGRAMS	139
APPENDIX II. MAPPING OF ECCENTRIC SPHERES TO CONCENTRIC SPHERES	154
APPENDIX III. USE OF MAPPED ECCENTRIC DATA IN DESIGN APPLICATION	163
BIBLIOGRAPHY	167

LIST OF TABLES

Table	Page
3.1. Dimensions of Cylindrical Bodies	37
4.1. Pertinent Mapped Dimensions and Parameters . . .	57
4.2. Comparison of Eccentric Sphere Results with Existing Concentric Sphere Empirical Correlations	71
4.3. Empirical Constants and Deviations for Equations of the Form of (4.5), (4.6), (4.7), and (4.8)	76
4.4. Deviations of the Cylindrical Heat Transfer Correlations	110

LIST OF FIGURES

Figure	Page
3.1. Heat transfer apparatus	36
3.2. Interior of inner sphere.	39
3.3. Interior of inner cylinder.	40
4.1. Eccentric sphere heat transfer data for the 9.00 inch sphere, 350 cs fluid and all eccentricities.	58
4.2. Eccentric sphere heat transfer data for the 4.50 inch sphere, 350 cs fluid and all eccentricities.	59
4.3. Mapped gap thickness to radius ratio as a function of actual gap thickness to radius ratio with $e/(r_o - r_i)$ as a parameter.	61
4.4. Eccentric data for all spheres, 350 cs fluid and all eccentricities.	63
4.5. Eccentric data for all spheres, water, and all eccentricities.	64
4.6. Comparison of the mapped eccentric heat transfer data to the existing concentric sphere correlations for each individual fluid .	73
4.7. Comparison of all mapped eccentric heat transfer data to the overall correlation for the concentric spheres.	74
4.8. Heat transfer correlations for all of the eccentric data and each individual fluid. . . .	77
4.9. Overall heat transfer correlation for all of the eccentric sphere data.	78

Figure	Page
4.10. Temperature profile for the 7.00 inch sphere, water, $e/(r_o - r_i) = -0.5$, $\Delta T = 41^\circ\text{F}$, and $N_{PR} = 8.45$	82
4.11. Effect of ΔT on temperature profile for the 5.50 inch sphere, $e/(r_o - r_i) = -0.75$, $\Delta T = 31^\circ\text{F}$ and 15°F , and $N_{PR}^i = 8.7$ and 10.0	84
4.12. Temperature profile for 5.50 inch sphere, water, $e/(r_o - r_i) = -0.75$, $\Delta T = 31^\circ\text{F}$, and $N_{PR} = 8.7$	85
4.13. Temperature profile for the 9.00 inch sphere, water, $e/(r_o - r_i) = +0.75$, $\Delta T = 46^\circ\text{F}$, and $N_{PR} = 7.7$	87
4.14. Temperature profile for the 9.00 inch sphere, 350 cs fluid, $e/(r_o - r_i) = +0.25$, $\Delta T = 63^\circ\text{F}$, and $N_{PR} = 3224$	88
4.15. Temperature profile for the 9.00 inch sphere, 20 cs fluid, $e/(r_o - r_i) = -0.25$, $\Delta T = 58^\circ\text{F}$, and $N_{PR} = 254$	89
4.16. Temperature profile for the 4.50 inch sphere, 350 cs fluid, $e/(r_o - r_i) = -0.25$, $\Delta T = 62^\circ\text{F}$, and $N_{PR} = 3569$	91
4.17. Isotherm plot for the 5.50 inch sphere and $e/(r_o - r_i) = -0.75$	93
4.18. Isotherm plot for the 5.50 inch sphere and $e/(r_o - r_i) = 0$	94
4.19. Isotherm plot for the 5.50 inch sphere and $e/(r_o - r_i) = +0.75$	95
4.20. Isotherm plot for the 9.00 inch sphere and $e/(r_o - r_i) = -0.75$	96
4.21. Isotherm plot for the 9.00 inch sphere and $e/(r_o - r_i) = +0.75$	97

Figure	Page
4.22. Heat transfer data for the 7.00 inch cylinders and water	102
4.23. Heat transfer data for the 5.50 inch cylinders and water	103
4.24. Heat transfer data for the 4.50 inch cylinders and water	104
4.25. Cylindrical data for all cylinders and water.	106
4.26. Temperature profile for the 5.50 x 7.25 inch cylinder, water, $\Delta T = 25^{\circ}\text{F}$, and $N_{PR} = 9.65$	114
4.27. Effects of ΔT on temperature profile for the 5.50 x 7.25 inch cylinder, water, $\Delta T = 44^{\circ}\text{F}$ and 25°F , and $N_{PR} = 8.32$ and 9.65	116
4.28. Temperature profile for the 4.50 x 6.25 inch cylinder, water, $\Delta T = 34^{\circ}\text{F}$, and $N_{PR} = 8.96$	118
4.29. Temperature profile for the 5.50 x 9.00 inch cylinder, water, $\Delta T = 20^{\circ}\text{F}$, and $N_{PR} = 10.2$	120
4.30. Temperature profile for the 4.50 x 9.00 inch cylinder, water, $\Delta T = 33^{\circ}\text{F}$, and $N_{PR} = 8.98$	121
4.31. Isotherm plot for the 7.00 x 9.00 inch cylinder and water.	123
4.32. Isotherm plot for the 4.50 x 9.00 inch cylinder and water.	124
4.33. Isotherm plot for the 7.00 x 8.00 inch cylinder and water.	126
4.34. Isotherm plot for the 4.50 x 6.75 inch cylinder and water.	127
4.35. Isotherm plot for the 9.00 x 9.33 inch cylinder and water.	129

Figure	Page
A2.1. Original eccentric configuration	155
A2.2. Configuration as a result of the first mapping.	158
A2.3. Configuration as a result of the second mapping.	159
A2.4. Configuration as a result of the final mapping.	161

x

ABSTRACT

Natural convection heat transfer between isothermal vertically eccentric spheres and centrally located vertical cylinders and their isothermal spherical enclosure was experimentally investigated. Pertinent dimensionless parameters and variables utilized in the investigation were Rayleigh number, based on gap width, N_{RA} , Prandtl number, N_{PR} , eccentricity to gap width ratio, $e/(r_o - r_i)$, gap width to inner radius ratio, L/r_i , and aspect ratio, $H/2r_i$, and covered the following ranges:

$$4.7 < N_{PR} < 4148, \quad 4 \times 10^2 < N_{RA} < 9 \times 10^7, \quad 0.09 \leq L/r_i \leq 1.18$$

and $-0.75 \leq e/(r_o - r_i) \leq +0.75$ for the eccentric spheres;

$$6 < N_{PR} < 14, \quad 3.5 \times 10^3 < N_{RA} < 2.2 \times 10^8, \quad 1.14 \leq H/2r_i \leq 2.00$$

and $0.09 \leq \frac{r_o - r_i}{r_i} \leq 1.18$ for the vertical cylinder.

Examination of the experimental data showed that the eccentricity had a slight effect on the average heat transfer coefficient. The negative eccentricities were found to produce slightly higher average heat transfer coefficients than positive eccentricities. The largest eccentricities, either positive or negative, were also seen to produce heat transfer coefficients larger than the next lower eccentricity, i.e., the average heat transfer coefficient for $e/(r_o - r_i) = \pm 0.75$ > the average heat transfer coefficient for $e/(r_o - r_i) = \pm 0.50$, etc. Gap thickness to inner radius ratio, L/r_i , was also found to have an effect on the average heat transfer coefficient. The larger values of L/r_i were found to yield higher values of Nusselt number. An increase in the viscosity did tend to suppress this behavior, however, the same trend was still found to exist. Heat transfer correlations for each individual fluid, as well as an overall correlation, were obtained for the eccentric sphere configuration utilizing conformal mapping techniques to transform the eccentric sphere configuration. Temperature profiles at five angular locations ($\theta = 0^\circ, 40^\circ, 80^\circ, 120^\circ, \text{ and } 160^\circ$) were taken

and yielded some insight as to the flow behavior and heat transfer as a result of eccentricity. A negative eccentricity was seen to enhance the convective activity while a positive eccentricity seemed to suppress the convective activity. A multicellular flow field is postulated for the smallest diameter ratio configuration.

The experimental data for the cylinders were examined independently and showed that aspect ratio did have an effect on the average heat transfer coefficient. The smaller aspect ratios for each diameter ratio produced higher average heat transfer coefficients. Heat transfer correlations were obtained for each cylinder as well as an overall heat transfer correlation for all of the cylinders. Temperature profiles were taken and were enlightening as to the nature of the effect of aspect ratio and diameter ratio on the flow field. The larger aspect ratios for all diameter ratios seemed to curtail the convective activity while the smaller aspect ratios for all diameter ratios seemed to promote convective activity. A multicellular flow regime is postulated for the smallest diameter ratio cylinder investigated.

NOMENCLATURE

Symbol	Description
a, b, c, d	Characteristic physical dimensions; exponents in functional equations
A	Area
C	Constant
$C_{1\dots n}$	Constants in equation (4.9)
C_p	Fluid specific heat at constant pressure
D	Diameter; width of vertical enclosure
e	Base of natural logarithms (2.71828...); eccentricity
E	Voltage
f	Denotes function
F	Denotes function
g	Acceleration of gravity, 32.174 ft/sec ²
h	Length of straight cylindrical section
\bar{h}	Convective heat transfer coefficient (average, defined as $\bar{h} = q_{net}/A\Delta T$)
H	Height of vertical plate; total height of cylinder
I	Electrical current
ID	Inner body diameter
k	Fluid thermal conductivity
k_c	Equivalent thermal conductivity

Symbol	Description
k_{eff}	Effective thermal conductivity, $k_{eff}/k = qL/4\pi k(T_i - T_o)r_o r_i$
l	Overall cylindrical length, $l = H$
L	Distance between plates; gap thickness, defined as $L = (r_o - r_i)$; length of vertical enclosure
N_D	Characteristic physical dimension ratio, a/b
N_{GR_a}	Grashof number, $\rho^2 g \beta (T_i - T_o) a^3 / \mu^2$, a is replaced by any desired characteristic dimension
N_{NU_a}	Nusselt number, $\bar{h}a/k$, a is replaced by any desired characteristic dimension
N_{NU^*}	Modified Nusselt number, $N_{NU^*} = N_{NU} / (1 + L/r_i)$
N_{PR}	Prandtl number, $C_p \mu / k$
N_{RA_a}	Rayleigh number, $\rho^2 g \beta (T_i - T_o) a^3 C_p / \mu k$
N_{RA^*}	Modified Rayleigh number, $\rho^2 g \beta (T_i - T_o) L^4 C_p / \mu k r_i$
n	Exponent on functional notation equation
q	Heat transfer rate, total energy supplied to inner body
q_l	Heat transfer rate, losses
q_{net}	Heat transfer rate, net, $q_{net} = q - q_l$
r	Radius to a point between the inner and outer surfaces; dimensionless radius ratio, $r = (R - R_o) / (R_o - R_\theta)$
R	Radius to a point within the annulus

Symbol	Description
r_{avg}	Average radius, $r_{avg} = (r_i + r_o)/2$
r_e	Reading on dial caliper used in equation (3.6)
r_i	Radius of inner body
r_o	Radius of outer sphere
r_{ref}	Reference reading used in equation (3.6)
R_i	Mapped radius of inner sphere
R_θ	Distance from center of the enclosing sphere to the surface of the inner body along a $\theta = \text{constant}$ line
R_o	Mapped radius of outer sphere; radius of outer sphere as used in equation (3.7)
T_i	Temperature of inner body
T_o	Temperature of outer sphere
T	Temperature at some point between the inner body and the outer sphere
T_{am}	Arithmetic mean temperature
T_{vm}	Volumetric mean temperature
ΔT	Difference between inner body surface temperature and outer sphere surface temperature, $\Delta T = (T_i - T_o)$
u_3	Defined by equation (A2.7)
u_2	$u_2 = -u_3$
u_1	Defined by equation (A2.13)
u	Abscissa in w plane

Symbol	Description
v_3	Defined by equation (A2.7)
v_2	$v_2 = -v_3$
v_1	Defined by equation (A2.13)
v_{exp}	Value of experimental data
v_{eqn}	Value of equation
w_3	Defined by equation (A2.6)
w_2	Defined by equation (A2.11)
w_1	$w_1 = u_1 + iv_1$
w	Defined by equation (A2.15)
x_2	Defined by equation (A2.4)
x_1	Defined by equation (A2.3)
x	Defined by equation (A2.2)
x'	Defined by equation (A2.1)
X	Independent variable used in equation (2.29) and defined as $X = N_{RA} [1 - D_i/D_o]^{6.5}$
$X_{1...n}$	Independent variable used in equation (4.9)
y	Dependent variable used in equation (4.9); defined by equation (A2.2)
y'	Defined by equation (A2.1)
z	Defined by equation (A2.9)
α	Thermal diffusivity, $k/\rho C_p$
β	Thermal expansion coefficient

Symbol	Description
Γ	Dimensionless temperature ratio, $\Gamma = (T - T_o)/(T_i - T_o)$
μ	Dynamic viscosity of the fluid
ϕ	Functional notation
ρ	Fluid density
π	Ratio of circumference of circle to diameter, 3.1415927...
θ	Angular displacement, measured from the upward vertical axis
σ	Deviation
δ	Average percent deviation
η	Inverse relative gap width, $2r_i/(r_o - r_i)$

Symbol	Subscripts
am	Arithmetic mean
F	Freon-11
H	Based on height of plate
i	Inner body surface, at a point
l	Denotes losses
L	Based on distance between plates or gap thickness ($r_o - r_i$)
m	Mapped
o	Outer spherical surface
R	Inner radius
s	Stem
um	Unmapped
vm	Volume mean
θ	Based on angular position

CHAPTER I

INTRODUCTION

During the past fifty years, technology has advanced far beyond all its previous years. This occurrence has fostered many problems and yielded some developments almost too awesome and spectacular to comprehend. During the same fifty year period considerable attention has been given to the phenomenon of natural convection heat transfer from a body to an infinite atmosphere. However, many of the natural convection problems confronting modern technology are those of a body and its finite enclosure, and only a small amount of data exists for this case. Extrapolation of these existing data to new configurations not covered by the existing data has had to suffice for design criteria. Extrapolation is acceptable only when adequate data are not available, and then should be used with extreme caution.

Several papers dealing with natural convection to bodies within finite enclosures have been published in recent years in an effort to overcome the serious lack of data. These papers primarily deal with concentric cylindrical and spherical annuli, and the natural convection

phenomena which occur within these geometries have been quite well defined for Prandtl number range 0.7 to 4148 and for a wide range of diameter ratios and Grashof numbers. Unfortunately, these data are not enough to characterize natural convection within the many geometry variations possible, even with these simple configurations. There exists a need to extend these concentric configurations to ones with the inner body in an eccentric location and, as a further extension, to completely change the internal body shape. Absolutely no knowledge of the resulting flow field, heat transfer, or temperature profiles which might be encountered as a result of these changes is available. The existing data might be extrapolated in some manner to yield a prediction of these phenomena, but experimental verification attesting to its accuracy and effectiveness would be non-existent. Extrapolation of data to a different case is quite dangerous and often produces disastrous results when used to establish design criteria.

It might be appropriate to consider the manners in which a heat transfer prediction may be accurately made for a selected geometry. The first attempt might be an analytical solution of the governing equations and associated boundary conditions. It is immediately evident that

due to the non-linearity of the governing equations, any analytical solution will be extremely difficult and may, as in the case of Mack and Hardee [1], be severely limited in applicability as well as being quite difficult to employ. Numerical techniques can also be utilized to effect a solution, and attempts along these lines have been successful in accurately predicting occurrences and trends for simple geometries but are quite laborious and difficult to employ. Therefore, another method of dealing with the problem is considered -- an experimentally determined solution in the form of an empirical equation.

The purpose of the current study is to experimentally obtain information concerning natural convection heat transfer between an eccentrically located sphere and a vertical cylinder and their spherical enclosure; and to determine the temperature distributions that take place within these two geometric configurations. These new data should aid in extending the current data to include these two new configurations and perhaps yield the necessary insight to effect a correlation that will encompass more than one geometry. The temperature profiles to be taken will be helpful in describing the flow phenomena and the heat transfer that takes place within these two configurations.

The basis for the current study will be the recent work of Scanlan, Bishop and Powe [2] for concentric spheres. This work presents several heat transfer correlations -- one for each of the test fluids involved (air, water, Dow Corning 200 Fluid - 20 cs, and Dow Corning 200 Fluid - 350 cs) and a single equation for all four fluids. The Dow Corning 200 fluids are silicone base fluids, and the 20 cs and 350 cs designations refer to the kinematic viscosity in centistokes at 25°C. An attempt will be made in the current investigation to correlate the experimentally obtained data with the data for the concentric spherical case [2] whenever possible.

The overall goals of this study are thus:

(1) To obtain empirical relationships that will characterize the natural convection heat transfer taking place between the spherical enclosure and the inner body for a wide range of variation of the independent variables for the eccentric sphere configuration and the cylindrical inner body configuration. The eccentricity is defined as the vertical displacement of the horizontal centerline of the inner sphere relative to that of the enclosing sphere. It may be positive (upward) or negative but is confined to the vertical axis. The cylindrical inner body is defined

as a right circular cylinder with hemispherical ends. A concentric location of this inner body is defined as the centroids of the inner body and the enclosing sphere being coincident and the longitudinal axis of the cylinder being coincident with the vertical axis of the enclosing sphere. The heat transfer was measured for various eccentricities for a spherical body and for a concentrically located cylindrical body as a function of impressed temperature differential.

(2) To obtain temperature distributions within the gap as the temperature difference between the two bodies is varied for a wide range of the independent variables.

(3) To correlate the current data with those currently in existence [2] for the concentric spherical annuli.

The apparatus used to determine the heat transfer rates and the temperature profiles was constructed such that the independent variables included the temperatures of the two bodies; the size, shape, and location of the inner body; and the test fluid. The radial temperature profile can be determined at five angular locations starting with 0° (upward vertical axis) and spaced at 40° increments.

CHAPTER II

LITERATURE REVIEW

Considerable attention has been given to natural convection heat transfer over the last fifty years. The area which has received the most attention has been the case of convection from a body to its infinite surroundings. Other geometries that also received much attention were horizontal and vertical rectangular enclosures. The most recent contributions have been relative to convection from bodies to their finite enclosures with the geometries most often considered being concentric cylindrical and spherical annuli.

For clarity the discussion is presented in three parts. These are (1) horizontal and vertical rectangular enclosures (parallel flat plates), (2) concentric cylindrical annuli, and (3) concentric spherical annuli. The main topic of interest is concentric spherical annuli. However, the other geometries are presented for completeness and to demonstrate similarities between natural convection phenomena which occur in the various geometries.

The case of natural convection from a body to an infinite atmosphere will not be treated since this subject is

quite adequately covered in standard textbook references. Jakob [3] and Gröber, Erk, and Grigull [4] present very complete and informative reviews on natural convection heat transfer from a body to an infinite atmosphere. They also treat very adequately the topic of convection within vertical and horizontal enclosed spaces. The reader is referred to these sources for the case of a body to an infinite atmosphere and for a complete list of pertinent references for this situation.

Natural convection heat transfer within enclosures will be the general topic covered, and specific attention will be given to natural convection from bodies to a finite enclosure. In order to accomplish this, the introduction of some terminology at this point might be helpful. The study of the natural convection process involves both fluid mechanics and heat transfer considerations. This fact dictates that any characteristic parameters which describe the phenomena will be derived from a combination of these disciplines. The literature on natural convection generally agrees that the following dimensionless groups characterize the phenomena for finite enclosures:

$$N_{GR_a} = \frac{\rho^2 \beta \Delta T a^3 g}{\mu^2} \quad (2.1)$$

$$N_{PR} = \frac{C_p \mu}{k} \quad (2.2)$$

$$N_D = \frac{a}{b} \quad (2.3)$$

where "a" and "b" are characteristic dimensions, ΔT is a suitably defined temperature difference, N_{GR_a} is called the Grashof number based on "a", N_{PR} is the Prandtl number, and N_D is a dimensionless ratio of the characteristic dimensions. An additional dimensionless group, the Rayleigh number, N_{RA} , is often used in place of the Grashof number and is the product of the Prandtl and Grashof numbers:

$$N_{RA_a} = N_{PR} \cdot N_{GR_a} = \frac{g \beta a^3 \Delta T}{\alpha \mu} \quad (2.4)$$

When considering natural convection heat transfer within enclosures, the literature, in general, states that the heat transfer taking place can be determined in functional notation as

$$N_{NU_a} = \phi [N_{GR_a}, N_{PR}, N_D] \quad (2.5)$$

where

$$N_{NU_a} = \bar{h}a/k \quad (2.6)$$

This type of functional relationship can easily be verified from an examination of the governing equations and the appropriate boundary conditions.

Jakob [3] and Gröber, Erk, and Grigull [4] indicate that this functional relationship can take the final form

$$N_{NU} = C [N_{GR} N_{PR}]^n \quad (2.7)$$

for natural convection from a body to an infinite atmosphere and for either laminar or turbulent flow. In this expression and all subsequent expressions, the Nusselt number has the same characteristic dimension as the Grashof or Rayleigh number appearing in the expression. Therefore, the subscript on Nusselt number will be deleted in subsequent expressions. (2.7) is indicative of no explicit dependence of the correlation on the aspect ratio. Here, aspect ratio would be defined as the ratio of characteristic dimensions. Further, Jakob [3] and Gröber, Erk, and Grigull [4] define a pseudothermal conductivity, k_{eff} , first postulated by Beckman [3], which when combined in a ratio with the thermal conductivity of the fluid for pure

conduction, describes the relative increase of heat transfer due to convection. The k_{eff} term may be described physically as the thermal conductivity necessary to conduct the same amount of heat as actually transferred by convection and conduction combined. Therefore, it is immediately seen that k_{eff}/k has a lower limit of 1. The same dimensionless variables and the same functional relationships associated with Nusselt number hold for k_{eff}/k and take the functional form

$$\frac{k_{\text{eff}}}{k} = \phi [N_{\text{GR}}, N_{\text{PR}}, N_{\text{D}}] \quad (2.8)$$

HORIZONTAL-VERTICAL-RECTANGULAR ENCLOSURES

Now consider natural convection heat transfer between horizontal and vertical enclosures. Jakob [3] gives expressions for heat transfer based on the data of Mull and Reiher which for horizontal air layers reduced from the form of the equation (2.6) to

$$\frac{k_{\text{eff}}}{k} = 0.195 N_{\text{GR}_L}^{1/4} \quad \text{for } 10^4 < N_{\text{GR}_L} < 4 \times 10^5, \quad (2.9)$$

and

$$\frac{k_{\text{eff}}}{k} = 0.068 N_{\text{GR}_L}^{1/3} \quad \text{for } N_{\text{GR}_L} > 4 \times 10^5 \quad (2.10)$$

For air contained between vertical plates, Jakob [3] gives the following equations:

$$\frac{k_{\text{eff}}}{k} = 0.18 N_{\text{GR}_L}^{1/4} \left(\frac{H}{L} \right)^{-1/9} \quad \text{for } 2 \times 10^4 \leq N_{\text{GR}_L} \leq 2 \times 10^5, \\ \text{and } 10.6 \leq \frac{H}{L} \leq 42.2 \quad ; \quad (2.11)$$

$$\frac{k_{\text{eff}}}{k} = 0.065 N_{\text{GR}_L}^{1/3} \left(\frac{H}{L} \right)^{-1/9} \quad \text{for } 2 \times 10^5 \leq N_{\text{GR}_L} \leq 11 \times 10^6, \\ \text{and } 10.6 \leq \frac{H}{L} \leq 42.2 \quad . \quad (2.12)$$

Here, H is the height of the plates and L is the distance between them. These expressions for both horizontal and vertical enclosures were much simpler than those of Mull and Reiher.

Globe and Dropkin [5] used mercury, water, and silicone fluids in studying heat transfer in liquids confined between horizontal plates heated from below. The work covered large ranges of Prandtl number, 0.02 to 8750, and Rayleigh number, $1.51(10)^5$ to $6.76(10)^8$. They arrived at the following correlation:

$$N_{NU} = 0.069 (N_{RA})^{1/3} (N_{PR})^{0.074} \quad (2.13)$$

Here all properties are evaluated at the arithmetic mean temperature of the two plates, and Nusselt and Rayleigh number are based on the distance between the plates. An extension of this work was carried out by Dropkin and Somerscales [6]. They studied the heat transfer between parallel plates at various angles of inclination with the horizontal for the same fluids as Globe and Dropkin. Their findings were in agreement with those of Globe and Dropkin [5]. They had the same form of equation including exponents on the Rayleigh and Prandtl numbers. The constant in front of the equation did, however, vary as a function of the angle of inclination from 0.069 for $\theta = 0^\circ$ to 0.049 for $\theta = 90^\circ$. The Prandtl number range was 0.02 to 11,560 and the Rayleigh number range was 5×10^4 to 7.17×10^8 , which represents somewhat of an extension to the previous investigation [5]. Landis [6], in commenting on the investigation of Dropkin and Somerscales [6], stated that their results indicate the correctness of the conclusion that, for natural convection flows in enclosures, Nusselt number correlations are particularly insensitive to geometry, boundary conditions, and flow regimes. Eckert and

Carlson [7] utilized a Mach-Zender interferometer to investigate the flow and temperature profiles in a long vertical rectangular duct for air. The heat transfer coefficients were then evaluated on the basis of the temperatures obtained. For the boundary layer region, they propose the following expression for an average Nusselt number based on the height of the plate:

$$N_{NU} = 0.119 (N_{GR})^{0.3} \quad (2.14)$$

They further proposed another correlation based on the distance between the plates. This expression is

$$N_{NU} = 0.119 (N_{GR})^{0.3} \left(\frac{L}{H}\right)^{0.1} \quad (2.15)$$

Batchelor [8] carried out an analytical solution for the problem of vertical walls. He was able to predict temperature and velocity profiles and, from these data, evaluate a Nusselt number. This work has been qualitatively verified by Eckert and Carlson [7] and produced the following expression for the heat transfer for small to moderate Rayleigh number, based on distance between plates:

$$N_{NU} = \frac{L}{D} + \left(\frac{2\gamma - 1}{720}\right) N_{RA} \text{ for } N_{RA} < 3 \times 10^4, \quad (2.16)$$

where γ is a constant usually taken to be 1. For large

values of Rayleigh number,

$$N_{NU} = 0.43 N_{RA_L}^{1/4} \left(\frac{L}{D} \right)^{3/4} \quad (2.17)$$

Batchelor also set up the mathematical mechanism by which subsequent analytical attempts to solve the governing equations and associated boundary conditions for other geometries were made.

Poots [9] applied numerical techniques to the problem of vertical walls with conducting connecting strips. His findings were in good agreement with both those of Jakob [3] and Batchelor [8]. He found the heat transfer to be determined by

$$N_{NU} = 1 + 5.08 \times 10^{-8} N_{RA_L}^2 \text{ for } N_{RA_L} < 10^3, \quad (2.18)$$

and

$$N_{NU} = 0.16 N_{GR_L}^{1/4} \text{ for } N_{RA_L} \sim 10^4. \quad (2.19)$$

He also hypothesized that the expression for $N_{RA_L} \sim 10^4$ would probably hold for larger values of Rayleigh number.

This was demonstrated by Jakob [3] who gives

$$N_{NU} = 0.18 N_{GR_L}^{1/4} \left(\frac{H}{L} \right)^{-8/9} \text{ for } 2 \times 10^4 \leq N_{GR_L} \leq 2 \times 10^5, \quad (2.20)$$

which is essentially the same expression except for the

aspect ratio term.

Wilkes and Churchill [10] applied numerical techniques to a long rectangular channel with air as the enclosed fluid. Their results agreed well with those of Poots [9] but there was a discrepancy between the results and the equation reported by Jakob [3] and given previously. Their data [10] varied from 0 to 70% in excess of the values predicted by equation (2.20). The variation was attributed to the range of (H/L) used in determining equation (2.20) being considerably beyond the range of (H/L) used for the numerical solution.

Another numerical solution to the governing equations for closed vertical walls is that of Newell and Schmidt [11]. They found their results to be in good agreement with existing experimental data and gave the following relationships for heat transfer:

$$N_{NU} = 0.0547 N_{GR_L}^{0.397} \text{ for } \left(\frac{H}{L}\right) = 1 \quad (2.21)$$

$$N_{NU} = 0.155 N_{GR_L}^{0.315} \left(\frac{H}{L}\right)^{-0.265} \text{ for } 2.5 \leq \left(\frac{H}{L}\right) \leq 20 \quad (2.22)$$

Their range of Grashof number was 4×10^3 to 1.4×10^5 .

Elder [12, 13] performed both experimental and numerical investigations of this problem. He did not, as did

Eckert and Carlson, determine any Nusselt number relationships from his data. He did, however, check his numerical solution against both his experimental data and the data of Eckert and Carlson [7] for validity and found the numerical predictions to be comparable to the experimentally determined values. On the basis of his experimental study, he described various types of flow and temperature fields which are generally in agreement with those of other investigators.

CONCENTRIC CYLINDRICAL ANNULI

Natural convection heat transfer in concentric cylindrical annuli has received considerable attention in recent years. This geometry has been investigated for a wide range of fluids, Grashof numbers, and diameter ratios. It has been investigated analytically, numerically, and experimentally.

Beckman [3] investigated this configuration in 1931 for air, hydrogen, and carbon dioxide as the enclosed fluids for diameter ratios (D_o/D_i) of 1.2 to 8.1. His Grashof number range was 640 to 1.5×10^7 . He postulated an effective thermal conductivity as a correlating implement and, utilizing dimensional analysis in conjunction

with physical arguments, arrived at the functional relationship

$$\frac{k_{\text{eff}}}{k} = \phi \left[N_{\text{GR}}, N_{\text{PR}}, \frac{D_o}{D_i} \right] \quad (2.23)$$

Kraussold [3] in 1934 extended Beckman's data utilizing water and two kinds of oil. His experiments were carried out for diameter ratios, (D_o/D_i) , of 1.2 to 3.0 and Prandtl numbers from 7 to 4000. He used the gap thickness, $L = (D_o - D_i)/2$, as the characteristic length and arrived at the following expressions for heat transfer:

$$k_{\text{eff}} = 1 \text{ for } N_{\text{RA}} < 10^3, \quad (2.24)$$

$$k_{\text{eff}} = 0.11 N_{\text{RA}_L}^{0.29} \text{ for } 6.4 \times 10^3 < N_{\text{RA}_L} < 10^6, \quad (2.25)$$

$$k_{\text{eff}} = 0.40 N_{\text{RA}_L}^{0.20} \text{ for } 10^6 < N_{\text{RA}_L} < 10^8. \quad (2.26)$$

Liu, Mueller, and Landis [14] performed an experimental investigation with five sets of concentric tubes containing air, water, or one of two silicone fluids to obtain a Prandtl number range of 0.7 to 3672. It was again found that the heat transfer could be correlated in terms of k_{eff}/k . The resulting expressions were

$$\frac{k_{\text{eff}}}{k} = 0.135 \left[\frac{N_{\text{PR}}^2 N_{\text{GR}_L}}{1.36 + N_{\text{PR}}} \right]^{0.278} \quad (2.27)$$

where

$$3.5 \leq \log \left[\frac{N_{\text{PR}}^2 N_{\text{GR}_L}}{1.36 + N_{\text{PR}}} \right] < 8.0 \text{ for } 0.25 \leq \frac{L}{D_i} \leq 3.25$$

and

$$\frac{k_{\text{eff}}}{k} = 1.0 \text{ for } \log \left[\frac{N_{\text{PR}}^2 N_{\text{GR}_L}}{1.36 + N_{\text{PR}}} \right] < 3.0 \quad (2.28)$$

They also compared their data with those of Beckman and Kraussold. Beckman's data were considerably higher than values predicted by their correlation. This was attributed to Beckman's failure to end insulate his apparatus. Kraussold's data, however, followed the general trend of the correlation but, on the average, was about 10% below the predicted values.

An experimental investigation relative to simple and obstructed annuli was performed by Lis [15]. His work covered a Rayleigh number range of 4×10^4 to 4.7×10^{10} for diameter ratios from 2.0 to 4.0, with Prandtl number varying from 0.645 to 1.32. He found the relation given on the following page to correlate his data within $\pm 12\%$. The correlating expression for simple annuli is

$$\log \left(\frac{k_{\text{eff}}}{k} \right) = 0.0794 + 0.625 \log X + 0.0154 (\log X)^2, \quad (2.29)$$

where $X = N_{\text{RA}} \left[1 - \frac{D_i}{D_o} \right]^{6.5}$ and N_{RA} is based on the inner diameter. His data showed considerable discrepancy from the predictions of Kraussold. This was attributed to the possibility that the use of the gap thickness in evaluating Rayleigh number did not entirely compensate for all the geometrical effects as suggested by Kraussold.

Another study, carried out at essentially the same time, was that of Grigull and Hauf [16]. They used a Mach-Zender interferometer to make their measurements. Their experimental data covered a Grashof number, N_{GR_L} , range from 320 to 716,000 at a Prandtl number of approximately 0.7 (air). The following equation was presented for the mean Nusselt number:

$$N_{\text{NU}_L} = [0.2 + 0.145 (L/D_i)] N_{\text{GR}_L}^{0.25} e^{-0.02(L/D_i)}$$

for $30,000 \leq N_{\text{GR}_L} \leq 716,000$,

and $0.55 \leq L/D_i \leq 2.65$. (2.30)

Their data were approximately 20% higher than the correlation of Liu, Mueller and Landis [14], but did agree with

those of Beckman and the predictions of Crawford and Lemlich [19].

Bishop [17], in a critique of the paper by Grigull and Hauf, utilized k_{eff}/k to obtain a simple correlating expression,

$$\frac{k_{eff}}{k} = 0.163 (N_{GR_L})^{0.2578} \text{ for } 5 \times 10^3 \leq N_{GR_L} \leq 7.16 \times 10^5,$$

$$\text{and } 0.32 \leq L/D_i \leq 2.65, \quad (2.31)$$

which correlated their data to -7.42% to +10.2%. This represented an extension in the range of applicable Grashof number and gap thickness to inner diameter ratio with the additional advantage of its being a simpler expression.

An analytical investigation for concentric cylinders was carried out by Mack and Bishop [18]. They utilized the technique set forth by Batchelor [8] and expanded the stream function and temperature in infinite series of powers of the Rayleigh number. They obtained the first three terms of the series for both the stream function and temperature. The solution, however, involves a large number of constants which must be determined sequentially. Utilizing the temperature and stream function solutions, they determined local and overall heat transfer in terms of

appropriate Nusselt numbers. Due to the fact that only the first three terms for both stream function and the temperature were obtained, the solution is necessarily limited to low values of Rayleigh number.

Numerical methods have also been applied to this problem by three investigators, [19], [20], and [21]. Crawford and Lemlich [19] utilized finite difference techniques in conjunction with a Gauss-Seidel iterative procedure to effect a solution to the concentric cylindrical case. They calculated both local and overall heat transfer effects through evaluation of the local and overall Nusselt number. Comparison of their data was made with those of Liu, Mueller, and Landis [14] and those of Beckman [3]. The agreement was fair for the data of Liu, et al, and within the scatter of the experimental data on which their correlations are based. The comparison with Beckman is much better. Therefore, quantitative as well as qualitative credibility has been established for this numerical model.

Abbott [20] also carried out a numerical solution to this problem utilizing iterative techniques requiring matrix inversions and multiplication, and his results compared quite well with the work of Crawford and Lemlich [19]. The matrix method was found to converge faster than the finite

difference technique for $N_{GR_L} (L/r_i)^3$ less than 6×10^5 to 2×10^6 . No definite value of the limit was established.

The latest numerical solution to this problem is that of Powe, Carley, and Carruth [21]. Their work is for air ($N_{PR} \sim 0.7$) and utilizes finite difference techniques to obtain a solution. The main concern of the effort was to numerically predict values of velocity, temperature, stream function, and Nusselt number near Rayleigh numbers where the flow will go from a steady condition into an unsteady condition for a wide range of inverse relative gap width η , (2.8 - 12.5). The existence of an unsteady condition was quite well documented, [14], [16], [17], [22], and [23]. The existing experimental data had been correlated to provide some insight to conditions for onset of the unsteady condition, but the data were sparse enough so that a well defined curve was not possible.

Powe, Carley, and Carruth [21] compared their results with the existing data and were reasonably successful in their attempts. They observed that the onset or existence of an unsteady condition did not noticeably affect the Nusselt number for any of the inverse relative gap widths considered. Temperature and velocity profiles were affected in accordance with the inverse relative gap thickness,

i.e., for larger inverse relative gap widths, there was a pronounced increase in the magnitude of the velocity components, and a distortion in the temperature profile was also noted for Rayleigh numbers above the value where the unsteady condition occurs.

CONCENTRIC SPHERICAL ANNULI

Heat Transfer

Until 1964, no experimental data existed for concentric spherical annuli. Since that time five investigations have been carried out [24], [25], [26], [27], and [2].

The first investigation was carried out by Bishop [24] for air ($N_{PR} \sim 0.7$) and a Grashof number range of 2×10^4 to 3.6×10^6 . Four inner spheres were utilized to provide diameter ratios of 1.25, 1.67, 2.00, and 2.50. Four separate correlations were determined -- one for each gap thickness to inner diameter ratio. These correlations are all based on gap thickness as the characteristic dimension and are

$$N_{NU} = 0.662 (N_{GR})^{0.217} \text{ for } 2 \times 10^5 \leq N_{GR} \leq 3.6 \times 10^6 ,$$

$$\text{and } \frac{L}{D_i} = 0.750 ; \quad (2.32)$$

$$N_{NU} = 0.1714 (N_{GR})^{0.291} \text{ for } 3.8 \times 10^5 \leq N_{GR} \leq 2 \times 10^6, \\ \text{and } \frac{L}{D} = 0.500 ; \quad (2.33)$$

$$N_{NU} = 0.068 (N_{GR})^{0.348} \text{ for } 2.3 \times 10^5 \leq N_{GR} \leq 1 \times 10^6, \\ \text{and } \frac{L}{D} = 0.333 ; \quad (2.34)$$

$$N_{NU} = 0.205 (N_{GR})^{0.235} \text{ for } 2 \times 10^4 \leq N_{GR} \leq 1.2 \times 10^5, \\ \text{and } \frac{L}{D} = 0.125 . \quad (2.35)$$

All properties in these and all subsequently appearing equations are evaluated at a volume weighted mean temperature defined as

$$T_{vm} = [(r_{avg}^3 - r_i^3) T_i + (r_o^3 - r_{avg}^3) T_o] / (r_o^3 - r_i^3) . \quad (2.36)$$

These correlations fit the data very well with the largest deviation being 8.2% and the average being approximately 5%. He also determined a single correlation equation

$$N_{NU} = 0.0122 e^{5.25(L/D_i)} (N_{GR})^{0.508} e^{-1.129(L/D_i)}, \\ \text{for } 0.333 \leq L/D_i \leq 0.750 \\ \text{and } 2 \times 10^5 \leq N_{GR} \leq 3.6 \times 10^6 . \quad (2.37)$$

This expression correlates all his data within the range

of deviations -9.3% to 7.7%. This correlating equation, while yielding very acceptable results well within the range of anticipated experimental accuracy, is quite formidable in its appearance. Therefore, a more attractive form was attempted:

$$N_{NU} = a (N_{GR})^b \left(\frac{L}{D_i} \right)^c \quad (2.38)$$

The expression of this form obtained was

$$N_{NU} = 0.332 (N_{GR_L})^{0.27} (L/D_i)^{0.52} ,$$

for $0.333 \leq (L/D_i) \leq 0.750$
and $2 \times 10^5 \leq N_{GR} \leq 3.6 \times 10^6$. (2.39)

His data deviated from this expression by -12.7% to +14.6%. The use of an equation with fewer empirical constants is quite desirable and a very accepted practice when the loss in accuracy is seen to be small.

Bishop, Mack, and Scanlan [25] utilized the work of Bishop [24] to attempt a different correlating technique. They defined an effective thermal conductivity, as suggested by Beckman [3], by means of the expression

$$\frac{k_{eff}}{k} = \frac{q_{net} L}{4\pi k \Delta T r_i r_o} \quad (2.40)$$

and further showed that k_{eff}/k can be written in terms of Nusselt number based on L as

$$\frac{k_{\text{eff}}}{k} = \frac{N_{\text{NU}}}{\left(1 + \frac{L}{r_i}\right)} = N_{\text{NU}*} \quad (2.41)$$

Then a correlation of the form

$$N_{\text{NU}*} = a (N_{\text{GR}})^b \quad (2.42)$$

was attempted. This type of equation has been seen in many previous discussions and indeed is sometimes quite successful as a correlation means. The resulting equation was

$$N_{\text{NU}*} = 0.106 (N_{\text{GR}_L})^{0.276} \quad \text{for } 0.25 \leq \frac{L}{r_i} \leq 1.50, \\ \text{and } 2 \times 10^4 \leq N_{\text{GR}_L} \leq 3.6 \times 10^6, \quad (2.43)$$

with a range of deviation of -13.4% to 15.5%. This equation presents a significant simplification over the previous one given by Bishop [24].

An analytical solution to the problem was carried out by Mack and Hardee [1] in much the same manner as that of Mack and Bishop [18] for concentric cylinders. They took the curl of the Navier-Stokes equations, which eliminates the pressure terms, and then introduced the stream function.

immediately satisfying the continuity equation. This left them with two equations to be solved, the vorticity equation and the energy equation, both in terms of stream function and temperature. The stream function and the temperature, the dependent variables, were expanded in an infinite series of Rayleigh numbers and the first three terms for both the stream function expansion and the temperature expansion were obtained, along with a large number of constants to be determined sequentially.

Due to the fact that only the first few terms were obtained, the solution is necessarily limited to low values of Rayleigh number. Their highest value of Rayleigh number was considerably below the lowest value obtained experimentally by Bishop, et al [25]. Even though direct comparison with experimental data was not possible, it was determined that the predictive trends were in the right direction, and therefore, qualitatively, the model is correct. To extend the applicable Rayleigh number range, more terms of the series must be obtained, and obtaining more terms of the series presents quite a laborious task.

The most recent study is that of Scanlan, Bishop, and Powe [2]. They extended the existing data of Bishop [24], ($N_{PR} \approx 0.7$), to include Prandtl numbers up to approximately

4148 by using water and two silicone fluids. The applicable range of Rayleigh number based on L was 1.3×10^3 to 5.8×10^8 with diameter ratios ranging from 1.09 to 2.81. They obtained a k_{eff}/k versus Rayleigh number correlation for each fluid, including air from Bishop's data, and then one for all four fluids combined. Utilizing k_{eff}/k as previously defined by Bishop, Mack and Scanlan [25], the correlation equations determined were

$$\frac{k_{\text{eff}}}{k} = 0.117 N_{\text{RA}_L}^{0.276} \text{ for } 1.4 \times 10^4 < N_{\text{RA}_L} < 2.5 \times 10^6,$$

$$\text{and } N_{\text{PR}} = 0.7, \quad (2.44)$$

$$\frac{k_{\text{eff}}}{k} = 0.033 N_{\text{RA}_L}^{0.328} \text{ for } 2.4 \times 10^4 < N_{\text{RA}_L} < 5.4 \times 10^8,$$

$$\text{and } 4.7 < N_{\text{PR}} < 12.1, \quad (2.45)$$

$$\frac{k_{\text{eff}}}{k} = 0.031 N_{\text{RA}_L}^{0.353} \text{ for } 2.4 \times 10^4 < N_{\text{RA}_L} < 9.7 \times 10^7,$$

$$\text{and } 148 < N_{\text{PR}} < 336, \quad (2.46)$$

$$\frac{k_{\text{eff}}}{k} = 0.056 N_{\text{RA}_L}^{0.330} \text{ for } 1.3 \times 10^3 < N_{\text{RA}_L} < 5.6 \times 10^6,$$

$$\text{and } 1954 < N_{\text{PR}} < 4148. \quad (2.47)$$

The equation that was determined for all fluids is based on a modified Rayleigh number which is the usual Rayleigh number multiplied by L/r_i . The equation given is

$$\frac{k_{eff}}{k} = 0.228 N_{RA*}^{0.226} \quad \text{for } 1.2 \times 10^2 < N_{RA*} < 1.1 \times 10^9$$

$$\text{and } 0.7 < N_{PR} < 4148 \quad . \quad (2.48)$$

These equations will therefore form the basis of comparison for the concentric and eccentric data.

Temperature Profiles

The discussion of the temperature profiles that exist within an enclosure during the process of natural convection will be limited in this section to those occurring within concentric spherical annuli. Temperature profiles for this configuration have been obtained both analytically and experimentally by a number of investigators, [24], [25], [2], and [1]. The experimentally determined profiles [24] have been utilized to check the validity of the analytical model, thereby establishing the credibility of the proposed model [1], at least qualitatively.

The first temperature profiles for the concentric spherical case were measured by Bishop [24] utilizing air as his test fluid. The temperature profiles were obtained

for selected temperature differences and angular positions for each of five diameter ratios. He found that all of the temperature profiles were quite similar in form except for the smallest L/r_i value whose temperature profiles were similar in form, but the ordering of the profiles was different. This fact was further emphasized when he examined the effect of impressed temperature difference on the temperature profile for three angular positions, 0° , 80° , 120° . The temperature profiles for these angular positions were found to be essentially independent of the impressed temperature difference for any given diameter ratio. Bishop plotted his data in terms of dimensionless radius and temperature ratios which were defined as

$$\frac{r - r_i}{r_o - r_i} \quad \text{and} \quad \frac{T - T_o}{T_i - T_o} \quad (2.49)$$

All temperature profiles exhibited the same characteristics and could be divided into five separate regions; 1) a very steep drop at the inner wall, 2) a gently curved inner sphere transition region, 3) a region of nominal slope, 4) a gently curved outer sphere transition region, and 5) a very steep drop at the outer wall. The steep drops at the inner and outer walls are attributable to the high rate of radial heat transmission. This condition is cer-

tainly due to the high velocities in the neighborhood of the walls. The transition regions are the physical joining of these steep drop areas to the low velocity central region. The central core would then be expected to have a shallow slope due to the low velocity.

These same general observations were made by Bishop, Mack, and Scanlan [25] for air as the test fluid. They describe five regions for temperature profile. They noted that the region immediately adjacent to the inner sphere has a much higher temperature gradient than does the region adjacent to the outer sphere. One reason offered for this is that the velocity immediately adjacent to the inner sphere is much greater than the velocity at the outer sphere.

It was also noted that for a gap to radius ratio, L/r_i , of 0.25 the temperature profiles did behave in a like manner to those just described but the profiles were ordered differently. The behavior of these temperature profiles could not be explained in terms of visually observed flow patterns for values of L/r_i of 0.19 and 0.37. This fact led to the postulation of a bicellular flow pattern in an effort to explain these anomalies in the temperature profile associated with this case. The bicellular

hypothesis was later re-evaluated to possibly be a multicellular flow condition by Scanlan, Bishop, and Powe [2]. They combined the previous work of Bishop [24] with their results for water and two silicone fluids. Their results indicated the existence of a temperature inversion for a variety of test conditions. The inversion was attributed to the high rate of angular convection of heat relative to radial transport, a condition quite possible at moderate to high temperature differences. Diameter ratios that were different in magnitude to any previously used were utilized, thereby expanding the range of applicable diameter ratio. The multicellular structure was hypothesized relative to the smallest gap to radius ratio, ($L/r_i = 0.09$). A large cell extending from the lower vertical axis to the upper region of the annulus and an arbitrary odd number of smaller cells filling the remainder of the annulus were postulated. It was further noticed that the size of the large cell apparently decreases in magnitude with increasing Prandtl number.

Mack and Hardee [1] also determined temperature profiles using their analytical model which has previously been discussed. They attempted to compare their results with the experimental results of Bishop, et al [25]. A

direct comparison could not be made due to a difference in Rayleigh number for each study. The highest Rayleigh number for which the expression was analytically valid was well below the lowest Rayleigh number experimentally obtained [25]. However, general trends were noted and compared. It was determined that the same ordering of the profiles relative to angular position was obtained. The large drops at both walls were not duplicated which could be due to the difference in Rayleigh numbers compared. The analytical model does, however, reproduce general trends observed experimentally, and therefore, the model can be said to have qualitative substantiation. As yet no experimental data are available at low enough Rayleigh numbers to effect a direct comparison.

The preceding discussion on the available literature points out the lack of data for natural convection heat transfer between a body and its finite enclosure. The purpose of the current study was to experimentally obtain additional information covering natural convection heat transfer between an eccentrically located sphere and a concentrically located cylinder and their spherical enclosure, and to determine the temperature distributions that exist as a result of the induced temperature differ-

ence within these two configurations.

CHAPTER III

EXPERIMENTAL APPARATUS AND PROCEDURE

EXPERIMENTAL APPARATUS

The heat transfer apparatus, Figure 3.1, consisted of either spherical or cylindrical inner bodies, an enclosing sphere, and a spherical water jacket. The spherical inner bodies combined with the enclosing sphere to yield values for L/r_i (relative gap thickness) of 0.09, 0.40, 0.79 and 1.18 with inner spheres of 9.00, 7.00, 5.50, and 4.50 inch diameters respectively. The cylindrical inner bodies had dimensions as shown in Table 3.1. The aspect ratio was defined as the ratio of cylindrical length to diameter. All of the inner bodies were fabricated from copper with an approximate thickness of 0.025 inches. The enclosing sphere was fabricated from 0.125 inch stainless steel hemispheres with an inner diameter of 9.828 inches.

The inner bodies were supported in the outer sphere by a stainless steel stem 0.50 inches in diameter and having a wall thickness of 0.065 inches. The stem was insulated on its lateral surface. The stem, in addition to providing support for the sphere, served as a support for electrical disk heaters and as a transfer tube for the power leads,

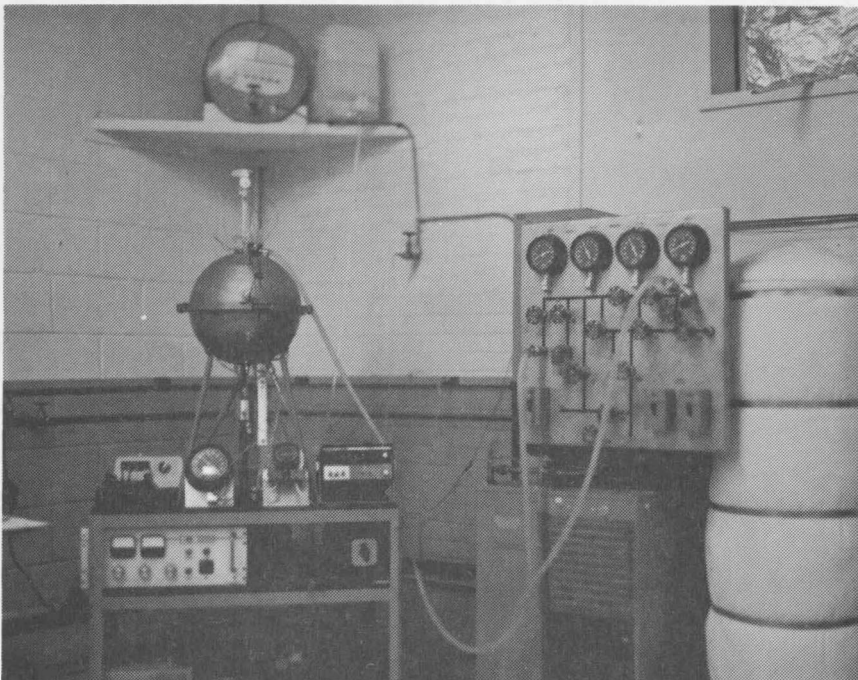


Figure 3.1. Heat transfer apparatus.

TABLE 3.1

DIMENSIONS OF CYLINDRICAL BODIES

DIAMETER D (IN)	CYLINDRICAL LENGTH h (IN)	OVERALL LENGTH l (IN)	ASPECT RATIO $\frac{h}{r_i}$
3.50	5.50 2.75	9.00 6.75	1.57 0.786
4.50	4.50 2.25	9.00 6.75	1.0 0.50
5.50	3.50 1.75	9.00 7.25	0.636 0.318
7.00	2.00 1.00	9.00 8.00	0.286 0.143
9.00	9.38	9.38	0.042

thermocouples, and liquid Freon-11. A constant temperature on the inner body surface was achieved by condensing Freon-11 vapor on the inner surface of the inner body. The saturation conditions of the Freon-11 were varied by changing the power input levels to electrical disk heaters contained within the body and located below the level of the Freon-11 liquid. The level of the Freon-11 liquid was controlled to some degree by a small stainless steel tube which acted as both a stand-pipe for venting during Freon-11 charging and as a means of measuring pressure within the inner body. The actual Freon-11 level within the body could be varied to some degree as a function of the ambient temperature and pressure within the body and the static head available from the Freon-11 reservoir. Figure 3.2 shows a typical arrangement of heaters, thermocouples, power leads, etc., within the sphere. A similar configuration was utilized on the cylinders, Figure 3.3. The number of heaters and their actual position, however, was a function of the size of the cylinder or sphere and, therefore, space available within the cylinder or sphere.

The surface temperature of the inner sphere was monitored by means of thermocouples placed in the seams of the two hemispheres prior to final assembly. Copper-con-

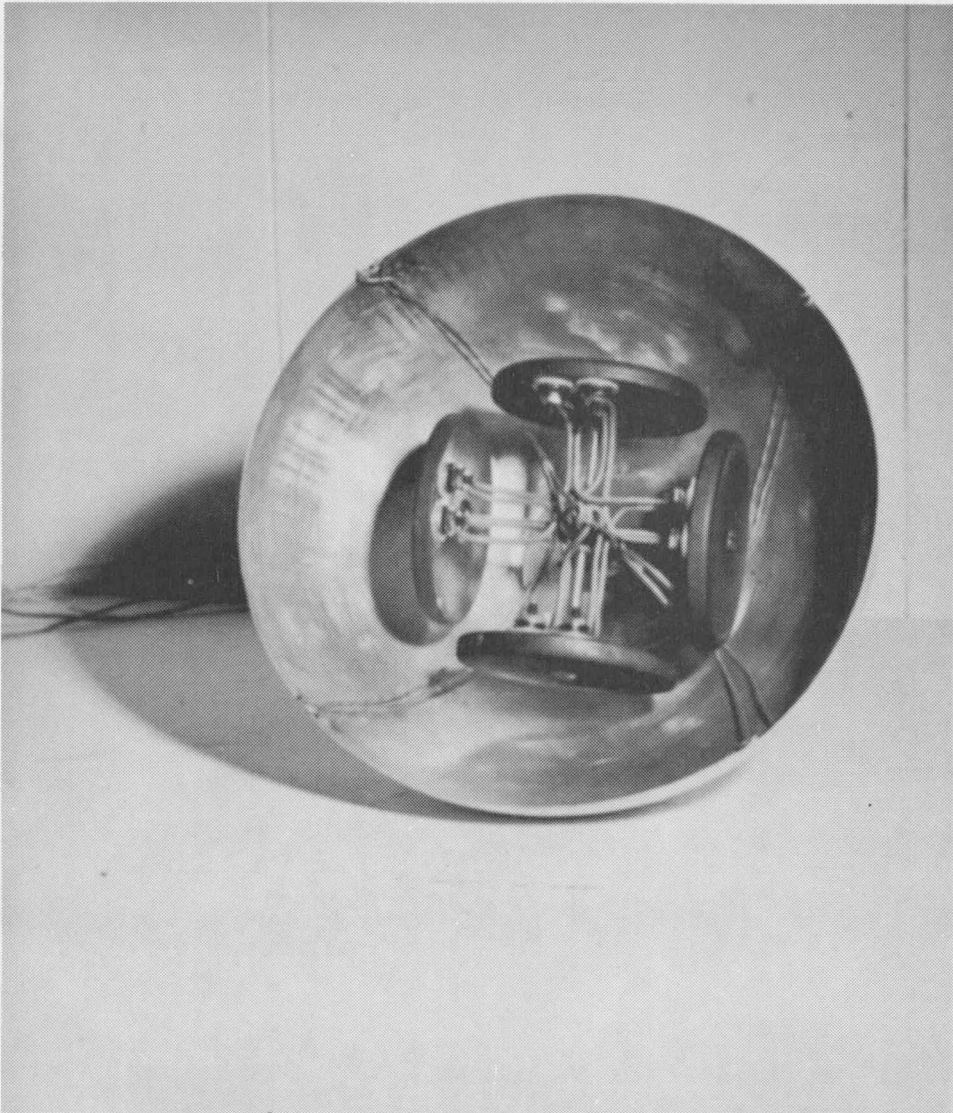


Figure 3.2. Interior of inner sphere.

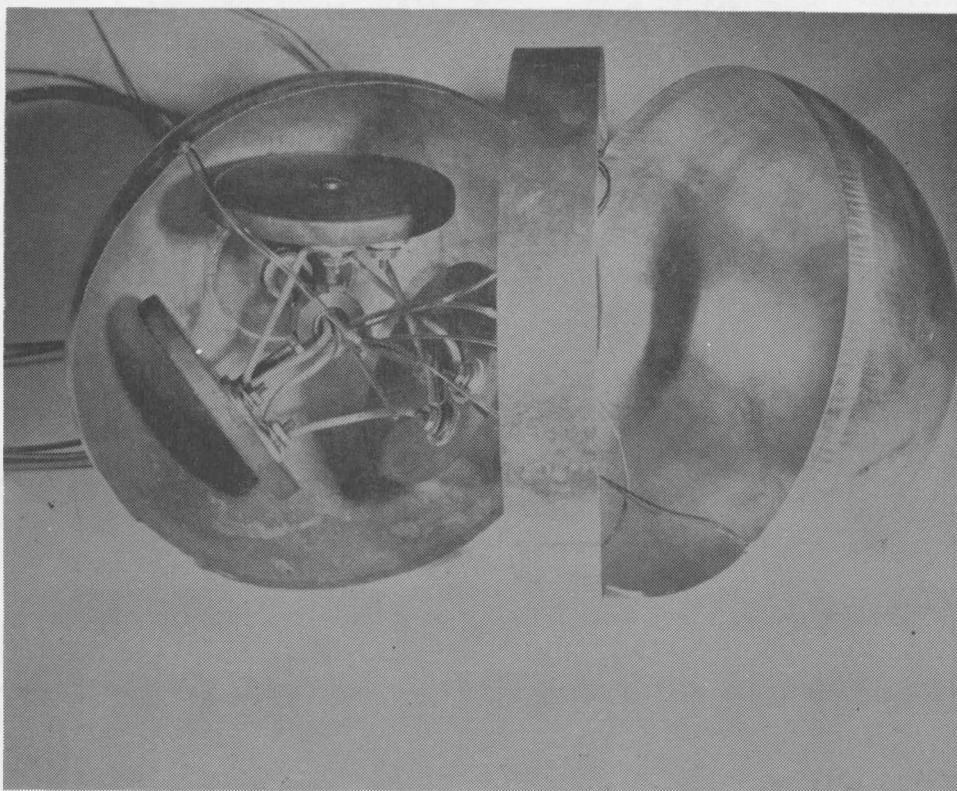


Figure 3.3. Interior of inner cylinder.

stantan thermocouples were utilized to monitor all temperatures. The surface temperatures of the cylinders were also monitored by means of thermocouples placed in both of the hemispherical seams and the vertical seam of the cylindrical section. The number of thermocouples within a cylinder was a function of its size and ranged from five to eight in number.

The outer (enclosing) sphere consisted of two stainless steel hemispheres which were joined together by an external flange. The flanged joint was sealed with an O-ring and held together with a flexible band to facilitate disassembly for changing of the inner body. The outer sphere was supported within the water jacket by a stainless steel spacer which was attached by screws to permit removal from the water jacket.

The water jacket was similar in design to the outer sphere in that it was fabricated from two stainless steel hemispheres which were joined together with an external flange and sealed with an O-ring. The hemispheres were 14 inches in diameter. The external flanges were held together by a flexible band to facilitate disassembly of the apparatus. The water which maintained the outer sphere at a constant temperature was introduced to the base and

withdrawn from the top through a manifold system. The water utilized to maintain the enclosing sphere at a constant temperature was contained within a closed system which included a reservoir, pump, and two chillers.

The inner sphere support tube passed through the enclosing sphere and the water jacket through O-ring seals and was connected to a small stainless steel reservoir. The reservoir allowed the emergence of power leads, thermocouples, standpipe, etc., through Conax fittings to provide leak-proof integrity of the system. The reservoir also housed the Freon-11 fill port. The reservoir rested on a threaded lead screw that allowed vertical positioning of the inner body. A stylus was also located on the reservoir as the position reference. A scale was located beside the reservoir so that the inner body could be accurately positioned vertically relative to the enclosing sphere at some predetermined location.

The thermocouple probes which were used to obtain the temperature profile data were fabricated from 24 gauge copper and constantan wires and inserted in 15 gauge fully hardened stainless steel hypodermic tubing and filled with epoxy cement around the wires to form a leak free probe. All thermocouple junctions were of the exposed

type. Each probe extended through the spherical water jacket and enclosing sphere and was long enough to traverse all the way to the inner body regardless of its location relative to the geometric center of the enclosing sphere. Movement and position of the probe was monitored by a specially modified dial caliper graduated in thousandths of an inch. O-rings and special fittings located at each sphere surface were used to seal around the probes. The probes were positioned at 40° increments starting at 0° (upward vertical axis) and extending to 160° for a total of five probe positions. The probes were placed in only one vertical plane, based on previous work [24] which indicated the presence of axisymmetric temperature profiles for stable flow patterns.

EXPERIMENTAL PROCEDURE

The desired inner body was selected and placed within the apparatus. All physical connections, such as plumbing, electrical power, and thermocouple leads, were made. The enclosing sphere and the spherical water jacket were installed and secured. The bottom four thermocouple probes were inserted in their respective locations, and a hollow tube was inserted in the zero degree location. The hollow tube was inserted just far enough into the enclosing sphere such that the annulus could be completely filled. The test fluid transfer tube was installed, and the reservoir containing the test fluid was placed on a shelf considerably above the apparatus, such that the annulus would fill via gravity flow. The zero degree thermocouple was then inserted into position after test fluid was physically spewing out of the hollow hypodermic tube. The Freon-11 fill and vent valves were then opened and the inner body was allowed to fill until a steady stream of Freon-11 was present in the vent line. Freon-11 flow was then terminated by securing the fill and vent valves.

The inner body was then placed in the desired location. This was accomplished by using the stylus located on the reservoir and adjacent scale. The inner body was

lowered and raised to its extreme upper and lower locations, where the inner body physically hit the enclosing sphere, and the scale readings recorded. For central or concentric locations, the inner body was placed at a position one half the difference between the two readings noted on the scale. For eccentric locations (spherical inner body), the predetermined location was accordingly set. These locations were $\pm 0.25L$, $\pm 0.5L$, and $\pm 0.75L$, where L (gap thickness) is equal to one half of the difference of the two recorded scale readings for the extreme locations.

The system was then ready for operation. This was initiated by energizing both the D.C. power supply, to the desired power level, and the chilling unit. The system was allowed to reach thermal equilibrium prior to recording data.

Upon reaching the condition of thermal equilibrium the following data were recorded:

- (a) Inner-body surface temperatures
- (b) Heater voltage and current
- (c) Inlet water temperature
- (d) Outlet water temperature
- (e) Run number

These data constituted those necessary to determine the desired heat transfer results.

Temperature profiles were taken at selected temperature differences (low, intermediate, and high). A temperature profile was obtained in the following manner. The temperature probe was located on the inner body. This was ascertained by observing electrical continuity between the temperature probe and the inner body on an ohm meter. The temperature probe was then withdrawn in small increments and the temperature measured, thereby determining the temperature as a function of radial position. Each of the five probes was set on the inner sphere and withdrawn incrementally and individually in this manner. The incremental withdrawal was made utilizing a specially modified dial caliper capable of measuring 0.001 inch increments. The temperature probes were constructed to be very stiff in an effort to resist bending in the presence of the internal flow or upon striking the inner body. Heat transfer data as previously described were taken immediately before and immediately after each traverse to aid in determining any variation in temperature conditions for the inner body and enclosing sphere existing during the temperature traverse. The normal variation was less than

1°F for the high temperature difference runs and less than a quarter of a degree F for the low temperature difference runs. The thermocouple probes, when not being used, were withdrawn to the surface of the enclosing sphere and therefore did not interfere with the reading taken during a traverse.

A data reduction program, written for the Sigma 7 Xerox Data Systems digital computer, was utilized to reduce the raw data and return the data in the desired form for further treatment as required or desired. A complete listing of this computer program is found in Appendix I. The previously mentioned experimental data for the establishment of the heat transfer rate were then converted within the computer program to the proper form for the determination of the heat transfer. The geometric and other physical variables affecting the heat transfer were pre-established for any given series of heat transfer runs. These were the experimental fluid, diameter of the inner sphere or cylinder, diameter of the outer sphere (always the same constant value), eccentricity (spherical geometry), and the length of the cylinder.

All of the thermocouple data were converted from millivolt readings to degrees Fahrenheit by the data re-

duction program. These temperature data were then utilized in the following manner. The inlet and outlet water temperatures were arithmetically averaged and became the temperature of the outer sphere. The variation in the inlet and outlet water temperatures was normally less than 0.5°F. The inner-body surface temperatures were averaged and became the inner-body temperature. The normal variation in the inner-body temperatures was less than 1°F for the spheres and approximately 10% of the temperature difference ($T_i - T_o$) for the cylinders. The inner-body temperature was always larger than the outer-sphere temperature and the difference between the two is the temperature difference that is the driving potential for heat transfer. The treatment of the experimental data involved the evaluation of thermal and physical properties of the experimental fluids which had to be evaluated at some suitable reference condition. Previous experimental efforts, [24], [2], have indicated that such a reference is satisfactorily yielded by a volume mean temperature, T_{vm} , which is defined by equation (2.36) as

$$T_{vm} = \frac{[(r_{avg}^3 - r_i^3) T_i + (r_o^3 - r_{avg}^3) T_o]}{(r_o^3 - r_i^3)} \quad (3.1)$$

This is physically interpreted as the average temperature obtained by treating the fluid from the outer wall to the midpoint of the fluid annulus as being at the temperature of the outer wall and that from the midpoint of the fluid annulus to the inner wall as being at the temperature of the inner wall. This relationship and definition were employed herein. An additional reference temperature was also employed. This was an arithmetic mean temperature defined as

$$T_{am} = \frac{T_i + T_o}{2} \quad (3.2)$$

The required thermal and physical properties are evaluated at the previously discussed volume weighted mean and arithmetic mean temperatures in function subprograms. These function subprograms also involved expressions that represent a best fit of the property data for the specific fluid. In the case of the two silicone fluids, the property data for the curve fit were supplied by the manufacturer. The water data were taken from published information.

The heater voltage and current were utilized to obtain the total amount of energy supplied to the inner body through the following relationship:

$$q = EI. \quad (3.3)$$

This heat transfer quantity was then corrected for losses. Since the fluids utilized are opaque to radiation, a correction for radiation loss was not required. Therefore, the only losses considered are the heat losses from the support stem. The lateral surface of the stem was insulated, and, therefore, convective losses from this surface were minimal and were not considered. The heat loss that was considered and subsequently deducted from the heat input to the system was that of conduction down the stem. This was arrived at in the following manner. The product of thermal conductivity of the stem and the Freon-11 and their respective areas were utilized in the one-dimensional steady-state Fourier conduction equation,

$$q_1 = \frac{(K_S A_S + K_F A_F)}{L} \Delta T, \quad (3.4)$$

with the gap thickness as the material thickness and the temperature difference (inner body to outer body) as the driving potential. The difference between the total amount of energy supplied to the inner body and this heat loss quantity was taken to be the net heat transfer from the inner body to the enclosing sphere. The average natural convection heat transfer coefficient at the inner surface

was then evaluated utilizing the net heat transfer, the driving potential, and the surface area of the inner body in Newton's law of cooling which is

$$\bar{h} = \frac{q_{\text{net}}}{A\Delta T} \quad (3.5)$$

The inner body surface was utilized in equation (3.5) from a purely arbitrary point of view. The fact that the $\bar{h}A$ product is a constant immediately allows the evaluation of the average heat transfer coefficient at the outer surface, once the inner one is known, since both areas are known.

Temperature Distribution Data

The experimental data for the temperature distribution within the annulus were taken at five angular positions (0° , 40° , 80° , 120° , and 160°) as a function of radial position within the annulus. All of these data were in the form of millivolt readings for specified positions. These data were input to a digital computer program written for the Sigma 7. A complete listing of this program and attendant subroutines is found in Appendix I.

Inlet and outlet water temperatures and surface temperatures, taken immediately preceding and after each probe traverse, were treated within the program to estab-

lish average values of the inner and outer wall temperatures during that particular probing. The same function subprogram employed in the heat transfer data reduction program for the establishment of temperatures was utilized to establish the temperatures from the recorded millivolt readings for all temperature data taken during an entire temperature profile run. The temperatures and corresponding radial positions were subscripted variables in the data reduction program so that they could be stored and specifically called for as required.

The actual radial position of any given point was determined in the following manner. The outer body was used as the reference datum. The radial distance from the outer body to the inner body as a function of inner-body diameter and eccentricity (spheres) had been predetermined geometrically. The value indicated on the dial caliper with the probe totally withdrawn to the wall of the outer body was recorded as the reference value, r_{ref} . Usually some convenient value, such as 0.000 or in some cases 1.000, was selected. The diameters of the beads on the end of the thermocouple were measured and determined to be 0.020 inches. The radial position was determined by the program utilizing the following equation:

$$R = R_o - (r_e - r_{ref}) + 0.020 \quad , \quad (3.6)$$

where R = the radius, R_o = radius of the outer body, r_e = reading on dial caliper, and r_{ref} = reference value. The radial position of the inner body surface relative to the center of the enclosing body at each of the five angular probe positions was also determined within the program. This allowed the construction of a dimensionless radius according to the expression

$$r = \frac{R - R_\theta}{R_o - R_\theta} \quad , \quad (3.7)$$

which ranges from 0 to 1 in magnitude. R is the radius at some intermediate point within the annulus, R_θ is the distance of the inner body surface from the geometric center of the enclosing body at a given angular location ($\theta = \text{constant}$), and R_o is the radius of the outer body.

Dimensionless temperatures were also constructed according to the expression

$$\Gamma = \frac{T - T_o}{T_i - T_o} \quad , \quad (3.8)$$

where T is the recorded temperature at some given point, and T_i and T_o are the temperatures of the inner body and

outer body respectively. These data, along with the actual radius and temperature at a point, were output for each radius and temperature recorded.

CHAPTER IV

DISCUSSION OF RESULTS

This chapter is presented in sections, one for the discussion of the experimental results for the eccentric spheres, and one for the discussion of the experimental results for the concentric cylinders. These sections involve the comparison of the results of that particular geometry with the existing empirical correlations for heat transfer in the concentric sphere case whenever possible. In addition, since the raw experimental data for the concentric sphere configuration are available, these data and the data for the eccentric sphere are combined to gain an overall correlation that involves more than one physical configuration.

Each of the sections for the eccentric spheres and concentric cylinder bodies treats the temperature distribution results in a sub-section.

ECCENTRIC SPHERES

Heat Transfer Data

One of the goals of the study was to determine the effects of eccentricity on the heat transfer. This was

the reason for selecting six eccentric positions for each sphere, which are indicated in Table 4.1. The eccentric experimental data were reduced in terms of the arithmetic mean temperature, equation (3.2), and the actual inner sphere radius. The experimental data for each sphere and fluid for all eccentricities were treated individually in an effort to emphasize the effects, if any, of eccentricity on the heat transfer coefficient. The data were compared by plotting Nusselt number versus Grashof number, both being based on the radius of the inner sphere. Certain behavior was apparent, and all the data for each sphere and fluid exhibited the same general trends, which is depicted by Figures 4.1 and 4.2. Here, each eccentricity is represented by a different symbol as noted in the individual figures. A close check of the data on a much enlarged graphical scale, showed that there is an 11 percent spread between the ± 0.75 eccentricities on Figure 4.2 and an 18 percent spread between them in Figure 4.1. The average error due to the experimental apparatus was determined to be approximately 13 percent. Therefore, spreads of these magnitudes within the data is conceivable. The data for the negative eccentricities were noted to always be higher than the data for the positive

TABLE 4.1

PERTINENT MAPPED DIMENSIONS AND PARAMETERS

ID (ACTUAL) (IN)	ID (MAPPED) (IN)	L/r_i (MAPPED)	ECCENTRICITY (IN)	ECCENTRICITY
9.00	9.27	0.06	± 0.31	$\pm 0.75L$
	9.11	0.08	± 0.21	$\pm 0.5L$
	9.02	0.09	± 0.10	$\pm 0.25L$
7.00	7.86	0.25	± 1.06	$\pm 0.75L$
	7.32	0.34	± 0.71	$\pm 0.5L$
	7.08	0.39	± 0.35	$\pm 0.25L$
5.50	6.67	0.47	± 1.62	$\pm 0.75L$
	5.94	0.66	± 1.08	$\pm 0.5L$
	5.60	0.76	± 0.54	$\pm 0.25L$
4.50	5.82	0.69	± 2.00	$\pm 0.75L$
	4.98	0.98	± 1.33	$\pm 0.5L$
	4.61	1.13	± 0.67	$\pm 0.25L$

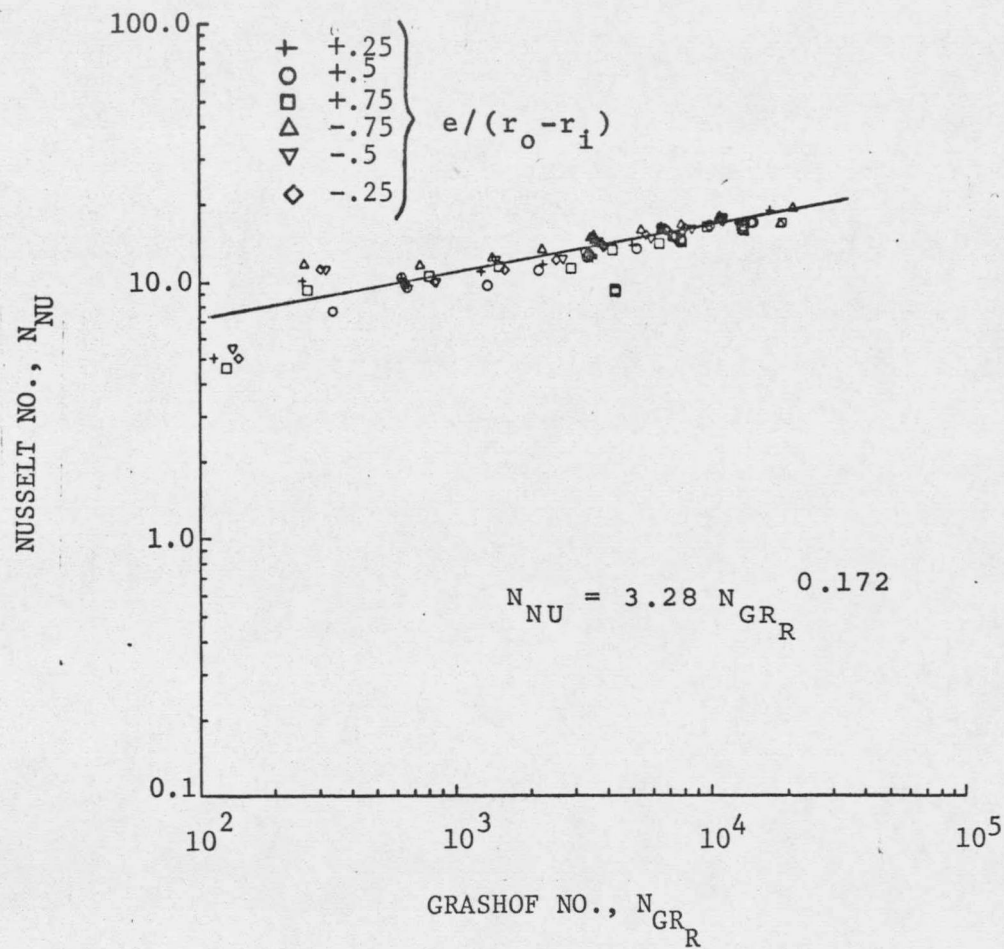


Figure 4.1. Eccentric sphere heat transfer data for the 9.00 inch sphere, 350 cs fluid and all eccentricities.

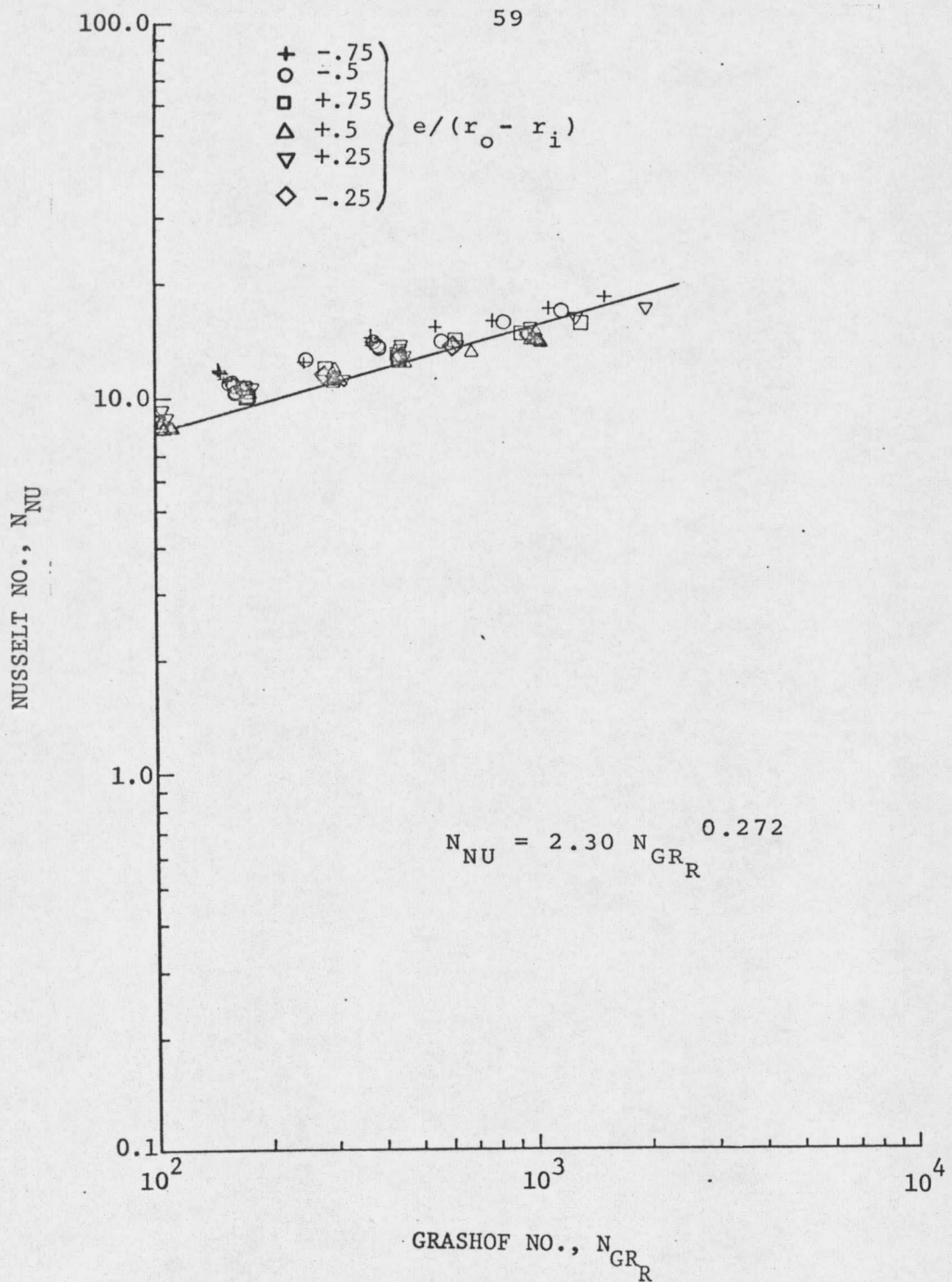


Figure 4.2. Eccentric sphere heat transfer data for the 4.50 inch sphere, 350 cs fluid and all eccentricities.

eccentricity of the same magnitude. The ± 0.75 eccentricity data were always higher in magnitude than the data of their associated ± 0.50 and ± 0.25 eccentricities, i.e., $-0.75 > -0.50$ data $>$ -0.25 data. A curve fit for each set of these data was carried out, and the resulting curve and equation for each set of data is shown in the respective figures. The equation for the data shown in Figure 4.1 fit the data with an average deviation of 9.7 percent, and the equation for the data shown in Figure 4.2 fit the data with an average deviation of 19 percent. A separate equation for each data set can be utilized to represent these data to within reasonable limits. Based on the above discussion, the eccentricity does appear to have an effect on the heat transfer coefficient, but a relatively minor one.

An interesting fact was observed from Figure 4.3. This figure was constructed utilizing conformal mapping techniques which are discussed in a later portion of the dissertation and in detail in Appendix II. Here it is seen that the same mapped gap width is obtained for either a positive or negative eccentricity of the same magnitude. Therefore, for the same inner and outer surface temperatures, the Grashof number obtained for either eccentricity

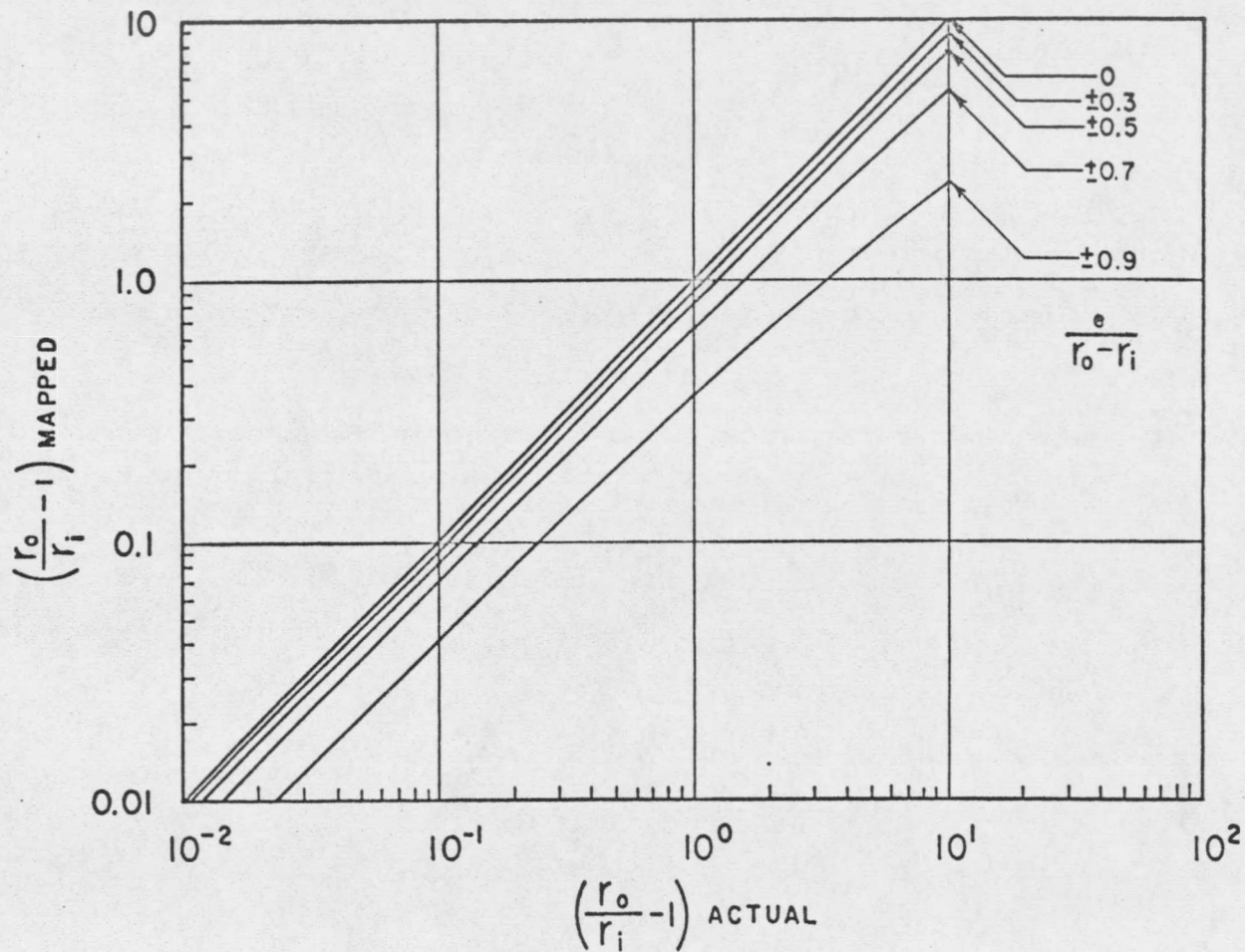


Figure 4.3. Mapped gap thickness to radius ratio as a function of actual gap thickness to radius ratio with $e/(r_o - r_i)$ as a parameter.

would be the same, and hence, the heat transfer coefficient would be the same. This would indicate that the mapping process removes the effect, even though minor, of eccentricity on the heat transfer coefficient.

There is also an effect of $(r_o - r_i)/r_i$ on the heat transfer coefficient which is exhibited in Figures 4.4 and 4.5. Due to the effect of eccentricity being minor as presented in the preceding discussion, all of the data involving all six eccentricities for a given sphere are depicted by one symbol. The effect of $(r_o - r_i)/r_i$ is clearly that the larger this ratio is for a given Grashof number, the higher the associated Nusselt number, as indicated by Figure 4.5 (Water). An interesting thing, however, is seen from Figure 4.4. This figure represents the 350 cs silicone fluid for all spheres and eccentricities. Here, it is seen that there is a similar effect of $(r_o - r_i)/r_i$ but, certainly, it is less prevalent than with the less viscous fluid, water. This same behavior was noted by Bishop [24] for concentric spheres and air as the test fluid. Bishop's data were indicative of a very great effect of $(r_o - r_i)/r_i$, much more so than is indicated by Figure 4.5 for water. This leads to the postulation that the more viscous fluids tend to damp out the

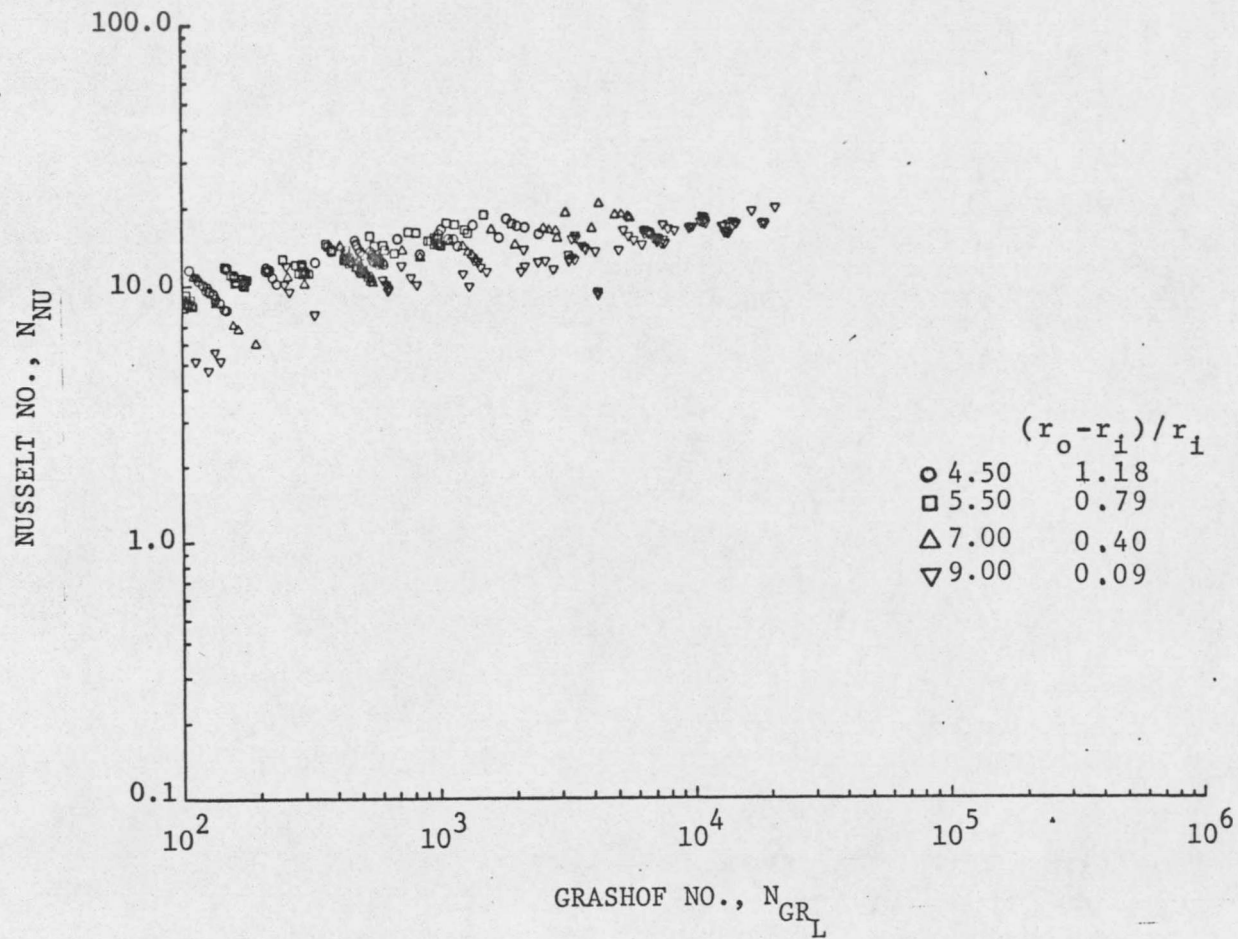


Figure 4.4. Eccentric data for all spheres, 350 cs fluid and all eccentricities.

